Erschienen in: Proceedings of the 26th European Photovoltaic Solar Energy Conference and Exhibition : the most inspiring platform for the global PV solar sector / Ossenbrink, H. et al. (Hrsg.). - Munich, Germany : WIP-Renewable Energies, 2011. - S. 1021-1024. - ISBN 3-936338-27-2
https://dx.doi.org/10.4229/26thEUPVSEC2011-2CO.13.3

CHARACTERIZATION OF DEFECT CLUSTERS IN COMPENSATED SILICON SOLAR CELLS

Dietmar Kohler, David Kiliani, Bernd Raabe, Sven Seren, Giso Hahn
University of Konstanz, Department of Physics, P.O. Box X916, 78457 Konstanz, Germany
Author for correspondence: dietmar.kohler@uni-konstanz.de, Tel.: +49 7531 88 3174, Fax: +49 7531 88 3895

ABSTRACT: The presence of defect clusters in multicrystalline silicon – not only in compensated silicon – can influence the electronic properties of solar cells. This is due to the interfered further crystallization and an insufficient passivation of the defects in these regions. Three-dimensional plots, based on hundreds of electroluminescence images, allow an improved analysis of the defect clusters' growth during crystallization. Furthermore, this allows vertical views from any angle which is otherwise only possible with destructive vertical cuts.
Keywords: Compensation, Defects, Electroluminescence

1 INTRODUCTION

Defect clusters in multicrystalline silicon are caused by thermal stresses during the crystallization process. Neighboring grains can grow with different orientations. This leads to strains at the grain boundaries where dislocations can nucleate [1]. So it is plausible that dislocations and grain boundaries are likely to occur in the same defect clusters. High concentrations of impurities within the crystal can also enable the formation of defect clusters. For this reason, the presence of clusters might be higher for compensated silicon. For high metal concentrations, metal precipitates can be formed at grain boundaries in dependence of the relative orientation of the neighboring grains which can implicate also decoration of dislocations [2]. This is supported by the roles of dislocations as so-called *pipe diffusions* for the transport of impurities [3] and as sites for internal gettering. So the defect clusters can influence the electronic properties of solar cells due to the modified further crystallization and an insufficient passivation of defects as well as formed metal precipitates.

Maps of the vertical formation of defects can help to evaluate the defect clusters' growth and their impact on solar cells. One method to obtain this information is the photoluminescence imaging of the bricks' surfaces or a cut close to the surface [4]. This is typically done at the edge of the ingot which is not intended for further cell processing. The alternative is to cut the whole brick in a vertical direction which means that the material is lost for the production of solar cells. This work presents a solution to this issue.

2 MATERIALS AND SOLAR CELL PROCESS

The following results are based on 15.6x15.6 cm^2 solar cells with screen-printed fired through SiN_x metallization. The feedstock that was used for this purpose was not cleaned in the Siemens process but in an alternative process which leaves a higher concentration of boron and phosphorus in the material. The term compensated Si refers to this and the fact, that further addition of dopants is needed to adjust the bulk resistivity as well as the type inversion level to receive a high wafer yield with acceptable resistivities. The wafers origin from a corner brick of this compensated Si ingot and were labeled consecutively from bottom to top. This enables a height dependent analysis of the whole brick. One of the main problems of compensated Si material is reported to be the possibly problematic breakdown behavior [5, 6] which is also considered here.

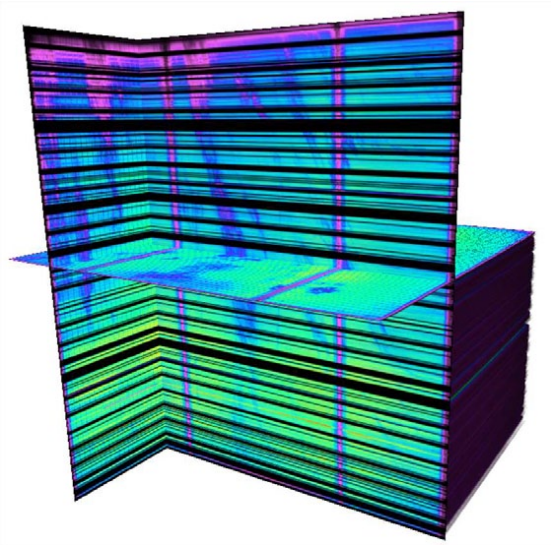

Figure 1: A three-dimensional plot, here based on 300 EL images under forward bias (20 mA/cm^2) of 6 inch solar cells, allows arbitrary vertical views of the inside of a brick without the need for destructive vertical cuts. The horizontal resolution is 152 µm/pixel, the vertical resolution 340 µm/pixel.

3 CHARACTERIZATION

IV measurements were performed under forward and reverse bias. Spatially resolved measurements were achieved by means of illuminated lock-in thermography (iLIT) and electroluminescence (EL) under forward bias (3 and 20 mA/cm^2) and reverse bias (-10 V).

The EL images under forward and reverse bias of solar cells from the whole p-type part of the selected corner brick were aligned and assembled on top of each other according to their original position in the brick. Missing solar cells were taken into account with empty substitutes. The resulting three-dimensional (3D) plots were assembled with the Zeiss software *AxioVision* in combination with several image editors. Two examples are shown in Fig. 1 and Fig. 3. The forward biased EL images were scaled globally and in color to provide both the shift of the defects as well as the decrease of intensity with ingot height. In contrast, the black and white EL images in Fig. 2 were scaled individually in order to focus on the position of the dark recombination active parts of each cell. The reverse biased EL images were measured at -10 V and a few of them were limited by a too high reverse current due to shunts. For the improvement of the depth perception, the breakdowns are

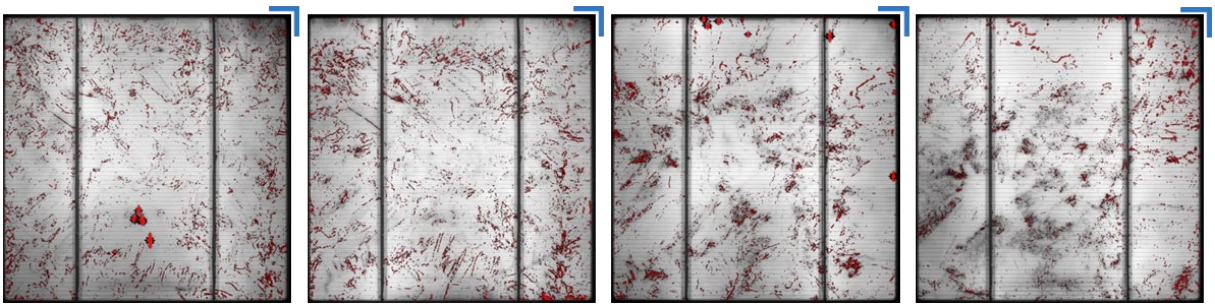

Figure 2: Many defect clusters shift inwards with proceeding crystallization, as shown in these EL images under forward bias of 3 mA/cm^2 for solar cells from increasing ingot heights (No. 027, 069, 245, 357 from left to right). The images under a reverse bias of -10 V are superpositioned in red. The ingot corner was located top right, as indicated by the blue symbol.

colorized in dependence of the position from red at the bottom to blue at the top. Thus, breakdown areas of same ingot height are represented in uniform colors. The resulting 3D image of the breakdowns can be seen in Fig. 3. A big advantage beside the fast measurement (here 5 s at 20 mA/cm^2) of the single images consists in the high spatial resolution of 150 µm per pixel for a 15.6x15.6 cm^2 solar cell compared to a similar plot of defects, done by Bergmann and shown in [7]. The vertical resolution is reduced by the wafer thickness of nearly 200 µm and the kerf loss due to wafer sawing as well as by the amount of missing wafers. The ingot corner can be seen backmost right in the image.

A few representative solar cells were cut into smaller cells in order to obtain spatial information in addition to the single values. After that, the IV measurements were repeated and the section images were assembled as described in our previous work [8].

4 RESULTS AND DISCUSSION

4.1 Three-dimensional plots

The 3D plot shown in Fig. 1 is based on 300 electroluminescence images under forward bias of 20 mA/cm^2. About 200 empty images were filled in the places of missing solar cells. This decreases the vertical resolution. The plot contains a combination of three perpendicular views. The dark blue patterns here show cluster formations. For increasing height, they shift towards the front left corner of the brick which is in the direction of the ingot center. The vertical purple lines are the positions of the bus bars. The visible color shift for increasing height can be explained by the decreasing open circuit voltage which is related to the increasing bulk resistivity (see Fig. 4) in this compensated material.

The EL images under reverse bias were assembled into a transparent 3D plot of the shunts within the brick, as shown in Fig. 3. One of the benefits of a rotatable 3D view is that the transformation of defect clusters and their influence on the breakdown behavior within the ingot can be clearly illustrated. Another possibility for further analysis offers the extraction of vertical views from any desired angle.

4.2 Shifting defect clusters

While the 3D plot is a good instrument for an analysis of these clusters which can range over wide parts of ingot height, the comparison of single EL images under forward bias as shown in Fig. 2 demonstrates the spatial distribution of the same clusters. With increasing ingot height, the clusters migrate from the ingot edge (in the images the top and right cell edges) towards the center, leaving behind a rather cluster-free edge zone. Stronger edge shunts are visible as thick horizontal lines in the 3D plot for EL under reverse bias in Fig. 3. These shunts were probably caused during the processing.

4.3 Compensation and local type inversion

In the blue-colored upper part of the 3D plot in Fig. 3, the breakdown sites are only visible at the former edge of the ingot. Detailed measurements in this part are shown in Fig. 4 and Fig. 5. For the cell No. 417 in Fig. 4, the electroluminescence image under forward bias shows that the clusters keep on shifting. But under reverse bias, no soft breakdown sites can be seen at the clusters close to the bottom left corner. This can be explained by the combination of two effects. First of all, different segregation coefficients of boron and phosphorus lead to a decrease of the net doping towards the upper part of the ingot. This means that the bulk resistivity increases as shown in Fig. 4. Because of the compensation, fewer free charge carriers are available for recombination. But this cannot explain the whole effect and especially not the still remaining breakdown sites at the edge of the ingot.

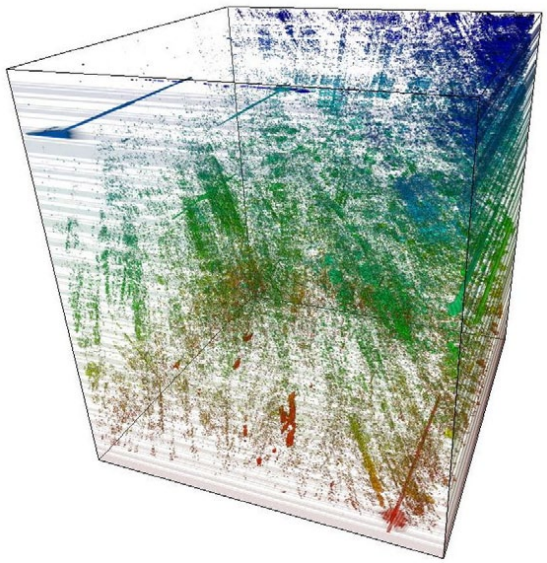

Figure 3: Three-dimensional transparent plot of the breakdown sites of the analyzed corner brick, made from single EL images under reverse bias of -10 V. The ingot corner is placed in the right backmost corner. The color gradient displays the height and is applied for an improved depth perception.

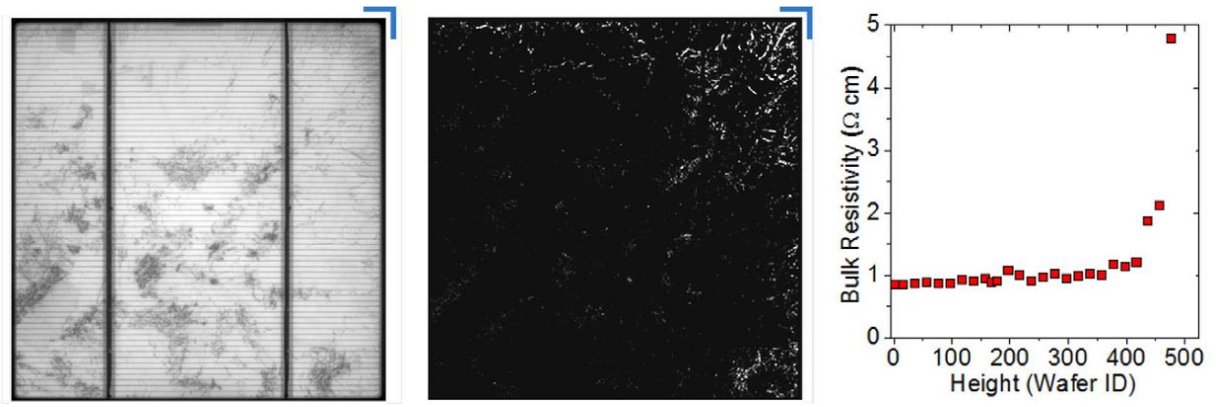

Figure 4: EL images under reverse (-10 V, left) and forward bias (center), and of the series resistance (right), each taken from the solar cell No. 417. The corner of the ingot was situated top right, as indicated by the blue symbol.

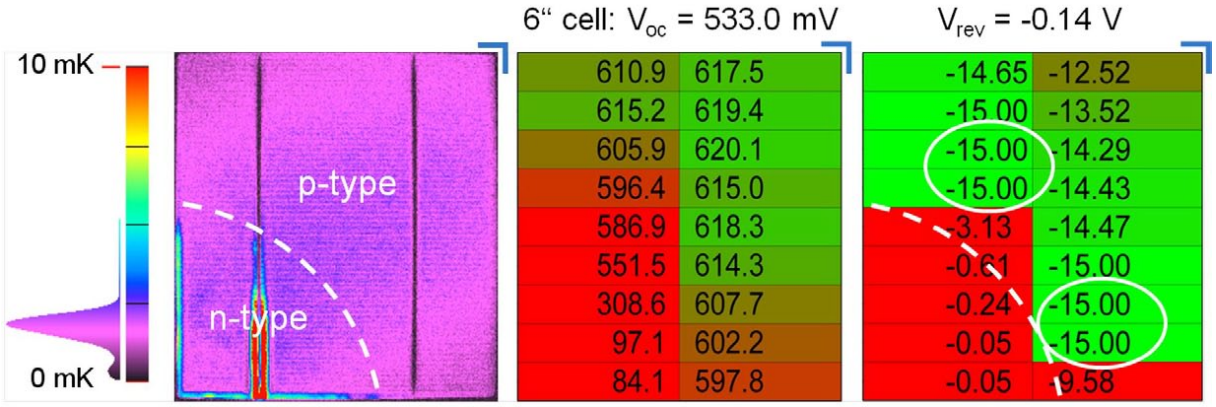

Figure 5: iLIT, V_{oc} map and breakdown voltage map of the solar cell No. 499 from the top of the ingot. It is assumed that the bottom left wafer part is already n-type due to the crystallization starting from the ingot edges (top and right).

The second effect is presented in Fig. 5. The solar cell No. 499 was positioned at the upper end of the p-type part. The iLIT image of this cell shows an increased temperature signal at the busbar and at the solar cell edge. It seems that the type inversion has already started in the bottom left corner of this cell. Similar effects were also reported by Haunschild et al. [4] and Kwapil et al.[9].

At this very high position in the p-type part, the EL measurement under reverse bias was not successful. So, this solar cell was cut into smaller subcells which were IV-measured under forward and reverse bias. The breakdown voltage for the large solar cell from this part was less than -0.2 V. However, the measurements of the small cut solar cells in Fig. 5 showed that this is caused only by the section in the bottom left corner which is closest to the ingot center, while the rest of the solar cell still has a very good breakdown quality. This can be explained by the assumption that the crystallization starts at the edge of the ingot. This is in accordance with the above mentioned decreased visible breakdowns towards the center of the ingot.

Since boron and phosphorus remain preferentially in the melt due to their segregation coefficients of 0.8 and 0.35, their concentrations are respectively higher in the center of the ingot at a certain height. Therefore, the low breakdown voltages are based on the partly commenced type inversion which probably appears first in the center of the ingot. Since the compensation effect decreases outwards from the ingot center, it can be concluded that the crystallization at a specific height starts at the ingot edge. This leaves the center part with a higher net doping and an earlier type inversion compared to the edge part at this height.

Spectrally resolved IQE measurements (not shown here) revealed a small increase of the effective diffusion length in the bulk in areas closer towards the ingot center, leading to a similar behavior for the short current density, which can be explained by the net doping effect.

The breakdown behavior of compensated silicon was reported to be worse than for electronic-grade silicon, caused by both the higher metal and net doping concentrations [5, 10]. As there is no general specification of compensated Si available, the impurity concentrations can differ a lot. The net doping concentration depends on the concentration already present in the feedstock and added contents of boron and phosphorus. For the material which was used in this experiment, the breakdown voltage measurements for the large solar cells were limited to 1 A/(156 cm)^2, while the small cut cells could be measured at up to 3 A/(156 cm)^2 due to the lower total current. Some solar cells from the lowest part of the brick are shunted, probably due to impurities from the crucible. For the rest of the brick, the reverse voltages for the large cells are better than -12 V and -13 V for the small cut cells. For increasing height, the reverse voltages follow the increasing base resistivity, according to Wagner’s results [10], until the type-inversion starts in parts of the wafer as shown in Fig. 5. Therefore, most of the solar cells made from this kind of compensated Si material shows a similar breakdown voltage as electronic grade multicrystalline solar cells [11].

5 SUMMARY

The rotatable three-dimensional plot allows a better visual perception of the objects than single images. In comparison to vertical cuts, the resolution is lower in dependence of the wafer thickness, kerf loss due to wafer sawing, and the quantity of missing wafers. But in contrast to the destructive vertical cutting of bricks, the presented method results in vertical views from any desired angle without damaging the material. Furthermore, the results of standard solar cell measurements can be included which are not available if the brick is cut vertically.

With electroluminescence imaging we used a fast measurement method for the creation of three-dimensional plots. In combination with a vertical coding as shown by Meyer Burger Technology AG [12], these 3D plots would also be easily available inline. No special material treatment or further measurement is necessary. The reverse biased images were assembled in a transparent plot. It reveals the distribution and drift of the breakdown locations associated with the defect clusters and can be executed for different breakdown voltages. Most of these compensated Si solar cells – except the highest and lowest ones – showed similar breakdown voltages as typical EG multicrystalline Si solar cells.

Three related effects were explained with several measurements in combination with these 3D plots: Most of the defect clusters shift towards the ingot center for increasing height. In the upper part of the brick, the signal of the electroluminescence under reverse bias vanished in the parts which are closer to the ingot center. Additionally, the topmost solar cell showed partial type inversion. These effects are assumedly caused by the inhomogeneous crystallization front. The crystallization starting at the edge leads to a higher dopant concentration and therefore an earlier type inversion in the ingot center.

6 OUTLOOK

The defect clusters vary in the magnitude of their impact on the electronic properties of the solar cells. Further experiments will compare different clusters with regard to their influences. In doing so, single clusters in the three-dimensional plots can be visually isolated by image editing and an adjustment of selective threshold and contrast.

The presented concept can be applied to any other measurement method that is fast enough for a high quantity of samples. First experiments were already done on photoluminescence measurements and will be continued.

7 REFERENCES

[1] B. Ryningen, K.S. Sultana, E. Stubhaug, O. Lohne, P.C. Hjemås, *Dislocation clusters in multicrystalline silicon*, Proc. 22nd EU PVSEC, Milan, 1086 (2007) 1086.

[2] T. Buonassisi, A.A. Istratov, M.D. Pickett, M.A. Marcus, T.F. Ciszek, E.R. Weber, *Metal precipitation at grain boundaries in silicon: Dependence on grain boundary character and dislocation decoration*, Appl. Phys. Lett. 89 (2006) 042102.

[3] M. Legros, G. Dehm, E. Arzt, T.J. Balk, *Observation of giant diffusivity along dislocation cores*, Science 319 (2008) 1646.

[4] J. Haunschild, M. Glatthaar, S. Riepe, S. Rein, *Quality control using luminescence imaging of mc-silicon solar cells from umg feedstock*, Proc. 35th IEEE PVSC, Honolulu (2010) 812.

[5] W. Kwapil, M. Wagner, M.C. Schubert, W. Warta, *High net doping concentration responsible for critical diode breakdown behavior of upgraded metallurgical grade multicrystalline silicon solar cells*, J. Appl. Phys. 108 (2010) 023708.

[6] O. Breitenstein, J. Bauer, P.P. Altermatt, K. Ramspeck, *Influence of Defects on Solar Cell Characteristics*, Solid State Phenomena (2009) 156.

[7] M. Rinio, *Untersuchung der prozessabhängigen Ladungsträgerrekombination an Versetzungen in Siliziumsolarzellen*, PhD thesis, TUBA Freiberg (2004) Fig. 3.5.

[8] D. Kohler, D. Kiliani, B. Raabe, S. Seren, G. Hahn, *Comparison of UMG materials: Are ingot height independent solar cell efficiencies possible?*, Proc. 25th EU PVSEC, Valencia (2010) 2542.

[9] W. Kwapil, M. Wagner, M.C. Schubert, W. Warta, *Cause of increased currents under reverse-bias conditions of upgraded metallurgical grade multicrystalline silicon solar cells*, Proc. 35th IEEE PVSC, Honolulu (2010).

[10] M. Wagner, B. Gründig-Wendrock, P. Palinginis, *Shunts, diode breakdown and high reverse currents in multicrystalline silicon solar cells*, Proc. 24th EU PVSEC, Hamburg (2009) 258.

[11] J. Bauer, J.-M. Wagner, A. Lotnyk, H. Blumtritt, B. Lim, J. Schmidt, O. Breitenstein, *Hot spots in multicrystalline silicon solar cells: avalanche breakdown due to etch pits*, physica status solidi (RRL) - Rapid Research Letters 3 (2009) 40.]

[12] P. Pauli, *Crystalline Silicon Wafering Technology, Current Status and Future Developments*, plenary presentation at 26th EU PVSEC, Hamburg (2011) *2BP.1.2.*